

Figure 8. X-ray diffraction pattern of the white powder scraped from the surface of a used catalyst pellet from the Ti (IV) cresylate Run.

process or service is to facilitate understanding and does not necessarily imply its endorsement or favoring by the U.S. Department of Energy.

#### LITERATURE CITED

Finkelman, R. B, *Scanning Electron Microscopy*, SEM, Inc., AMF O'Hare, IL, I, 143 (1978).  
 Given, P. H., R. N. Miller, N. Suhr, and W. Spackman, "Trace Elements in Fuel," *Adv. Chem. Ser.*, #141, American Chemical Society, Washington, DC (1975).  
 Gluskoter, H. Y., "Trace Elements in Fuel," *Adv. Chem. Ser.*, #141, American Chemical Society, Washington, DC (1975).  
 Kovach, S. M., L. J. Castle, and J. V. Bennett, "Deactivation of Hydrodesulfurization Catalysts under Coal Liquids. 2. Loss of Hydrogenation

Activity Due to Adsorption of Metallics," *Ind. Eng. Chem. Prod. Res. Dev.*, 17, No. 1, 62 (1978).

Makovskiy, L. E., S. S. Pollack, and F. R. Brown, "TiO<sub>2</sub> On and Around a Deactivated Hydrodesulphurization Catalyst," *Nature*, 288, 154 (1980).

Mason, B., L. G. Berry, *Elements of Mineralogy*, W. H. Freeman, San Francisco, CA, 306 (1968).

McGinnis, E. L., Div. Petroleum Chem., Preprints, 23(4), 1340 (1978), National Mtg., American Chemical Society, Miami Beach, FL (Sept., 1978).

Ocampo, A., and J. T. Schrodt, "Deactivation of Hydrodesulfurization Catalysts under Coal Liquids. 1. Loss of Hydrogenation Activity Due to Carbonaceous Deposits," *Ind. Eng. Chem. Prod. Res. Dev.*, 17, No. 1, 56 (1978).

*Manuscript received August 24, 1982; revision received November 17, and accepted December 14, 1982.*

# Dynamic Simulation of Azeotropic Distillation Towers

Algorithms are presented for integration of the stiff ordinary differential equations using an adaptive semi-implicit Runge-Kutta (ASIRK) integrator; an A-stable, single-step, noniterative algorithm with step-size control. Unusual open loop responses are encountered for simulations of azeotropic distillation towers and the results suggest two control variables. The results support the contention that one steady-state regime of operation is unstable.

**G. J. PROKOPAKIS and  
W. D. SEIDER**

Department of Chemical Engineering  
University of Pennsylvania  
Philadelphia, PA 19104

#### SCOPE

In 1978, we undertook to study the steady-state characteristics of azeotropic distillation towers (Prokopakis et al., 1981a). Our results demonstrated the extreme sensitivity of the steep con-

centration and temperature fronts to small changes in the boil-up rate, product recovery and purity, and the reflux ratio, and led to an algorithm to locate feasible specifications for the configuration in Figure 6a (Prokopakis and Seider, 1983). Furthermore, they showed three regimes of operation, which were

G. J. Prokopakis is presently at Columbia University.

simultaneously reported by Magnussen et al. (1979), who found an instance of instability for one of the regimes. These observations suggested the dynamic simulation studies reported herein, which reveal unusual responses to disturbances and support the observations of Magnussen and coworkers.

Many models for dynamic simulation of distillation towers have been reported, but these usually incorporate assumptions to simplify control algorithms. The typical assumptions of constant molal overflow and uniform relative volatilities throughout sections of the tower are not appropriate for the nonideal solutions in azeotropic towers. In these cases, it is necessary to include the MESH (Material balance, Equilibrium, Summation of mole fractions, Heat balance) equations for each tray. These comprise a large set of stiff ordinary differential equations (ODE's) that are integrated with semi-implicit or implicit integration formulas to prevent numerical instability.

To our knowledge, Ballard and Brosilow (1978) reported the first A-stable algorithm to integrate the stiff MESH ODE's with the step-size adjusted to give desired accuracy. They used a second-order, semi-implicit Runge-Kutta method, and observed that much of the Jacobian matrix is computed during function evaluation (with no extra computations). Subsequently, Boston and coworkers (1981), Callan and Holland (1980), and Sourisseau and Doherty (1980) developed other algorithms using the GEAR multistep integration method (Hindmarsh, 1974).

Ballard and Brosilow's observation that a good approximation to the Jacobian matrix is computed at no extra cost during function evaluation, led us to experiment with an adaptive method which we developed to improve upon the family of semi-implicit Runge-Kutta methods first introduced by Rosenbrock (1963). We obtained larger step sizes, approximately the same number of function evaluations and more Jacobian evaluations per step than with the GEAR method for systems of two and three ODE's (Prokopakis and Seider, 1981b); an observation confirmed by Bui (1981) with similar semi-implicit Runge-Kutta methods. Hence, since the MESH equations have the special property that the Jacobian matrix is computed during function evaluation, our algorithm should be more efficient. However, this was not tested due to the convincing evidence of Bui, the unavailability of a program to integrate the MESH equations using the GEAR method, and the extensive effort to program and test such a method.

In this paper, we briefly review the model for an azeotropic distillation column, with emphasis on the stiffness of its ODE's, and algorithms for integration of the MESH equations which incorporate generalized integrators such as the GEAR method. Then, we introduce a new integration algorithm using our ASIRK integrator, introduce a model for the dynamics of the decanter, and present unexpected open-loop responses to disturbances for a model of the configuration in Figure 6c.

## CONCLUSIONS AND SIGNIFICANCE

1. The new algorithms for integration of the MESH equations using the ASIRK integrator appear to be efficient and reliable for simulation of azeotropic distillation configurations. The algorithms are A-stable, single-step, noniterative, and do not require additional computations for the Jacobian submatrices. Furthermore, the equations are decoupled for integration and, for species with relatively small rates of change, re-evaluation of  $[I - ahJ]^{-1}$  can be avoided and, in some cases, integration is unnecessary across a time step.

2. Open-loop responses for dehydration of ethanol with benzene are unusual. The steep concentration and temperature fronts are observed to shift up and down the tower as expected. However, they initially move in the opposite direction due to "wash-out," an unexpected effect that increases with the hold-up. The term wash-out is justified to explain this inverse response and a similar response is noted in the simulations of

Peiser and Grover (1962). These theoretical results indicate the need for experimental verification.

3. A combination of disturbances can diminish the movement of the steep fronts, suggesting that azeotropic distillation towers can be controlled by adjusting the decanter bypass fraction and the reboiler heat duty.

4. A large increase in the feed flow rate shifts operation from a regime with alcohol and entrainer throughout the stripping section to one with appreciable water and negligible entrainer in the stripping section. In the transient, the profiles pass through an intermediate regime similar to that computed by solution of the MESH equations in the steady state. The regime has appreciable water throughout and entrainer on the upper trays of the stripping section and appears to be unstable. Hence, the observations of Magnussen and coworkers (1979) are supported.

## PRIOR WORK: DYNAMIC SIMULATION OF DISTILLATION TOWERS

There is an extensive literature on distillation dynamics, with emphasis on process control, tray hydraulics, and uncommon operating strategies, such as cyclic distillation. To our knowledge, the first simulation studies were reported for binary systems by Huckaba and coworkers (1963, 1965) and Luyben and coworkers (1964). Both obtained good agreement between simulation results and experimental measurements.

The earliest work on simulation of multicomponent distillation towers was limited by fixed-step integration algorithms that utilize unnecessarily small time steps throughout much of the range of integration or inefficient integration methods (Mah and coworkers, 1962; Waggoner and Holland, 1965; Distefano, 1968a,b; Howard, 1970). However, these authors formulated the mathematical models that are largely in use today. The usual nomenclature is shown in Figure 1, a schematic of a distillation tower, where the general Tray  $i$  has a feed stream, vapor and liquid sidestreams, and

heat transfer. Note that  $s_i^v$  is the fraction of vapor in the sidestream leaving Tray  $i$  and  $s_i^l$  corresponds for the liquid sidestream.

The models of Distefano (1968a), Howard (1970), Ballard and Brosilow (1978), and Boston and coworkers (1981) include the energy balance and share the following assumptions:

- (1) The vapor and liquid streams leave the trays at equilibrium.
- (2) The liquid on each tray is perfectly mixed.
- (3) The vapor hold-up on the trays is negligible.
- (4) The transportation delay of liquid and vapor between trays is negligible.
- (5) The temperature on each tray is uniform.

These lead to the following equations, beginning with the material balances for species  $j$  on Tray  $i$

$$\frac{d}{dt}(M_i x_{ij}) = (1 - s_{i+1}^L)L_{i+1}x_{i+1,j} + (1 - s_{i-1}^v)V_{i-1}y_{i-1,j} + F_i z_{ij} - L_i x_{ij} - V_i y_{ij} \quad i = 1, \dots, N \quad (1)$$

$$j = 1, \dots, C$$

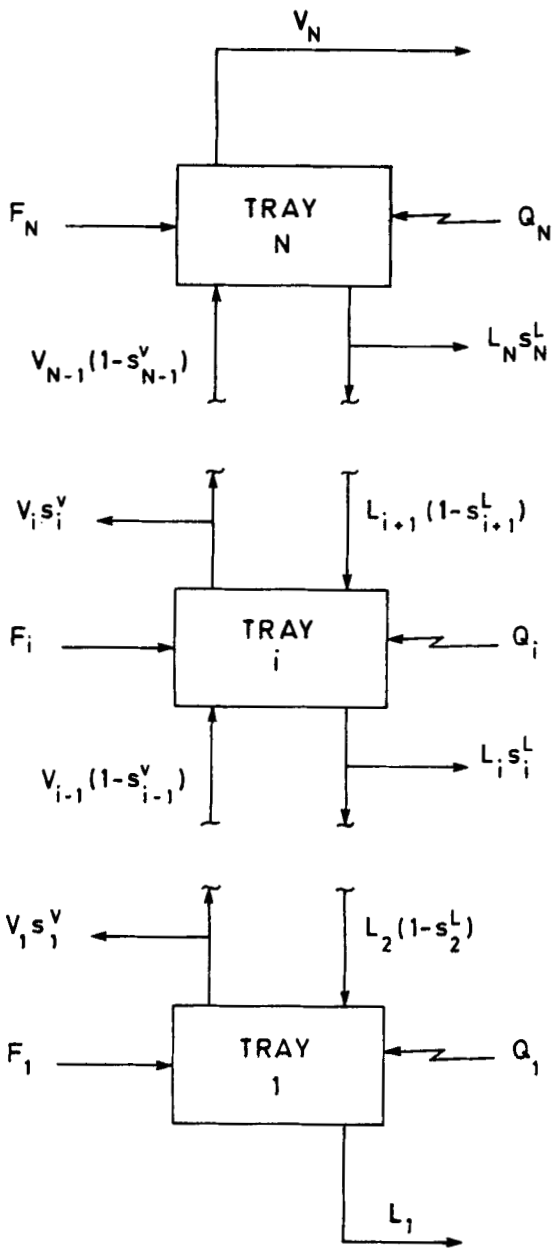


Figure 1. Schematic of a continuous distillation tower.

The overall mass balance on Tray  $i$  is:

$$\frac{dM_i}{dt} = (1 - s_{i+1}^L)L_{i+1} + (1 - s_{i-1}^V)V_{i-1} + F_i - L_i - V_i \quad i = 1, \dots, N \quad (2)$$

The equations that relate the compositions of vapor and liquid phases at equilibrium are:

$$y_{ij} = K_{ij}\{\underline{x}_i, \underline{y}_i, T_i, P_i\}x_{ij} \quad i = 1, \dots, N \quad j = 1, \dots, C \quad (3)$$

The energy balance on Tray  $i$  is:

$$\begin{aligned} \frac{d}{dt} (M_i h_i^L \{\underline{x}_i, T_i, P_i\}) &= (1 - s_{i+1}^L)L_{i+1} h_{i+1}^L \{\underline{x}_{i+1}, T_{i+1}, P_{i+1}\} \\ &+ (1 - s_{i-1}^V)V_{i-1} h_{i-1}^V \{\underline{y}_{i-1}, T_{i-1}, P_{i-1}\} \\ &+ F_i h_i^F \{\underline{x}_i, T_i, P_i\} + Q_i - L_i h_i^L \{\underline{x}_i, T_i, P_i\} \\ &- V_i h_i^V \{\underline{y}_i, T_i, P_i\} \quad i = 1, \dots, N \quad (4) \end{aligned}$$

The liquid hold-up on Tray  $i$  is:

$$M_i = \rho_i^L \{\underline{x}_i, T_i, P_i\} A_i (H_{w_i} + \Delta_{w_i}) \quad i = 1, \dots, N \quad (5)$$

where  $A_i$  is cross-sectional area of Tray  $i$ ,  $H_{w_i}$  is the weir height, and  $\Delta_{w_i}$  is the crest height of the liquid over the weir. Ballard and Brosilow (1978) use a form of the Francis weir formula to represent the tray hydraulics:

$$\Delta_{w_i} = 1.41 \left[ \frac{L_i}{\sqrt{g} \rho_i^L \{\underline{x}_i, T_i, P_i\} L_{w_i}} \right]^{2/3} \quad i = 1, \dots, N \quad (6)$$

where  $L_{w_i}$  is the weir length and  $g$  the acceleration due to gravity. However, Distefano (1968a), Howard (1970), and Boston and co-workers (1981) assume that  $\Delta_{w_i}$  is independent of  $L_i$ ,  $\rho_i^L$ , and  $L_{w_i}$ ; that is, a constant volume of hold-up exists on each tray.

In addition, the mole fractions for the vapor and liquid phases on Tray  $i$  sum to unity:

$$\sum_{j=1}^C x_{ij} = \sum_{j=1}^C y_{ij} = 1 \quad i = 1, \dots, N \quad (7)$$

There are  $N(C + 2)$  ODEs (Eqs. 1, 2 and 4), and  $N(C + 4)$  algebraic equations (Eqs. 3, 5-7); hence,  $N(C + 5)$  independent equations, since the overall mass balances depend on the remaining equations. There are  $N(3C + 15)$  variables and  $N(C + 10)$  specifications, with an appropriate set:  $F_i, \underline{x}_i, T_i^F, P_i^F, P_i, s_i^V, A_i, H_{w_i}, L_{w_i}, i = 1, \dots, N$ , and  $j = 1, \dots, C$ , plus  $Q_i, i = 2, \dots, N - 1, s_i^L, i = 1, \dots, N - 1$ , and three of the variables, reflux ratio ( $R$ ), boil-up ratio ( $R' = V_1/L_1$ ), bottoms flow rate ( $L_1$ ), boil-up rate ( $V_1$ ), reboiler heat duty ( $Q_1$ ), or condenser heat duty ( $Q_N$ ). Alternatively, tray pressures,  $P_i$ , can be computed as a function of the liquid head on the trays. Note that when constant volume hold-up is assumed, Eq. 6 and the variables  $L_{w_i}$  do not apply;  $\Delta_{w_i}$  is specified in place of  $L_{w_i}$ .

### Stiff ODE's

The Jacobian matrix of the MESH ODE's typically has small negative eigenvalues. Hence, in the rapid transient, immediately following a disturbance, the step size of an explicit integrator is not severely limited by a stability bound. However, as the rates of change decrease, the step size to achieve desired accuracy increases and the limitation gains significance; that is, the system stiffens and a stiff integrator (implicit or semi-implicit integrator without a stability bound) becomes more efficient. This variation in stiffness is examined for several physical systems by Seider and coworkers (1982).

Many authors use the stiffness ratio,  $SR = |Re\{\lambda\}|_{\max}/|Re\{\lambda\}|_{\min}$ , as a measure of stiffness. It successfully accounts for the spread in response times, but does not measure stiffness during the rapid transient where only  $|Re\{\lambda\}|_{\max}$  indicates whether an integrator with a stability bound must restrict its step size below that to give desired accuracy. Distefano (1968b) used SR and related it to the process variables. Although we prefer other measures of stiffness (Seider and coworkers, 1982), some of his development is useful. First, he combines Eqs. 1-13 to give:

$$\frac{d\underline{x}_j}{dt} = \underline{G}_j \underline{x}_j + \underline{d}_j \quad j = 1, \dots, C \quad (8)$$

where  $\underline{G}_j, j = 1, \dots, C$ , are tridiagonal matrices that approximate the Jacobian matrix,  $\underline{J}_j$ , for species  $j$ . He shows that the eigenvalues of  $\underline{G}_j, j = 1, \dots, C$ , are bounded as follows:

$$\left( \frac{L + KV}{M} \right)_{\max} \leq |\lambda|_{\max} \leq 2 \left( \frac{L + KV}{M} \right)_{\max}$$

where

$$\left( \frac{L + KV}{M} \right)_{\max} = \max_{i,j} \left( \frac{L_i + K_j V_i}{M_i} \right)$$

and, similarly,

$$\left( \frac{L + KV}{M} \right)_{\min} \leq |\lambda|_{\min} \leq 2 \left( \frac{L + KV}{M} \right)_{\min}$$

where

$$\left( \frac{L + KV}{M} \right)_{\min} = \min_{i,j} \left( \frac{L_i + K_{ij} V_i}{M_i} \right)$$

Hence, the eigenvalues of the system depend on the hold-ups, the range of  $K$ -values, and the circulation rates. Tyreus and coworkers (1975) observe that as purities approach unity with more trays, the mole fractions respond more slowly and  $|\lambda|_{\min}$  decreases more rapidly than  $|\lambda|_{\max}$ . After rapid transients, these systems are stiffer because the step-size to give desired accuracy increases more rapidly than that to give numerical stability with an explicit integrator. Similarly, for difficult separations (with large pinch zones), the MESH equations become stiffer as the response time increases.

### PRIOR WORK: ALGORITHMS FOR INTEGRATION OF THE MESH EQUATIONS

#### Ballard and Brosilow Algorithm

To our knowledge, the first distillation algorithm to use a semi-implicit or implicit method with step-size control was developed by Ballard and Brosilow (1978), who derived three working equations.

First, they combine Eqns. 1, 2 and 3 to give Eq. 8. Then, the overall mass balance (Eq. 2), Eq. 8, and the Francis weir formula (Eq. 6) are used to give:

$$\underline{\underline{M}}_L \frac{d\underline{\underline{L}}}{dt} = \underline{\underline{D}}\underline{\underline{L}} + \underline{\underline{E}}V - \underline{\underline{d}}_M \quad (9)$$

where  $\underline{\underline{M}}_L$  is the diagonal matrix of the derivatives of the holdup with respect to the liquid flow rate and  $\underline{\underline{D}}$  and  $\underline{\underline{E}}$  are bidiagonal matrices. It is assumed that the liquid density is a molal average of the densities of the pure species. The third equation is derived using the energy balance (Eq. 4) and the equilibrium equations (Eqs. 3) to give:

$$\underline{\underline{B}}\underline{\underline{L}} + \underline{\underline{C}}V = \underline{\underline{d}}_E \quad (10)$$

where  $\underline{\underline{B}}$  and  $\underline{\underline{C}}$  are bidiagonal matrices. Ballard and Brosilow assume that the liquid enthalpy is a molal average of the enthalpies of the pure species. However, when the heat of mixing is significant,  $\underline{\underline{B}}$ ,  $\underline{\underline{C}}$ , and  $\underline{\underline{d}}_E$  can be replaced by  $\underline{\underline{B}}^*$ ,  $\underline{\underline{C}}^*$ , and  $\underline{\underline{d}}_E^*$ , derived using analytical derivatives for  $\partial \ln \gamma_j / \partial T$ . Combining Eqs. 9 and 10

$$\frac{d\underline{\underline{L}}}{dt} = \underline{\underline{M}}_L^{-1}(\underline{\underline{D}} - \underline{\underline{E}}\underline{\underline{C}}^{-1}\underline{\underline{B}})\underline{\underline{L}} + \underline{\underline{M}}_L^{-1}(\underline{\underline{E}}\underline{\underline{C}}^{-1}\underline{\underline{d}}_E - \underline{\underline{d}}_M) \quad (11)$$

There are  $C + 1$  systems of  $N$  ODE's to be integrated for  $\underline{x}_j$ ,  $j = 1, \dots, C$ , and  $\underline{\underline{L}}$ . With new values of  $\underline{x}_j$  and  $\underline{\underline{L}}$  (during or after each time step),  $T_i$  and  $y_i$  are computed by solution of the bubble point equation on each tray:

$$\sum_{j=1}^C K_{ij}\{\underline{x}_j, \underline{y}_j, T_i, P_i\}x_{ij} = 1 \quad (12)$$

This algorithm is summarized in Figure 2. It solves Eqs. 1-7 accurately, except when molal average densities do not apply.

Given  $\underline{\underline{x}}_n$ ,  $\underline{\underline{y}}_n$ ,  $\underline{T}_n$ ,  $\underline{\underline{L}}_n$ ,  $\underline{V}_n$

1. Calculate  $\underline{x}_{n+1}$ ,  $\underline{\underline{L}}_{n+1}$  by integration of:

$$\frac{d\underline{x}_j}{dt} = \underline{\underline{C}}_j \underline{x}_j + \underline{\underline{d}}_x_j, \quad j = 1, \dots, C$$

$$\frac{d\underline{\underline{L}}}{dt} = \underline{\underline{M}}_L^{-1}(\underline{\underline{D}} - \underline{\underline{E}}\underline{\underline{C}}^{-1}\underline{\underline{B}})\underline{\underline{L}} + \underline{\underline{M}}_L^{-1}(\underline{\underline{E}}\underline{\underline{C}}^{-1}\underline{\underline{d}}_E - \underline{\underline{d}}_M)$$

2. Solve for  $\underline{\underline{V}}_{n+1}$

$$\underline{\underline{V}}_{n+1} = \underline{\underline{C}}^{-1}[\underline{\underline{d}}_E - \underline{\underline{B}}\underline{\underline{L}}_{n+1}]$$

3. Solve bubble point equation for

$$T_{i,n+1}, \underline{y}_{i,n+1} \quad i = 1, \dots, N$$

4. Let  $n \leftarrow n + 1$

Figure 2. Ballard and Brosilow algorithm.

Given  $\underline{\underline{x}}_n$ ,  $\underline{\underline{y}}_n$ ,  $\underline{T}_n$ ,  $\underline{\underline{L}}_n$ ,  $\underline{V}_n$

1. Calculate  $\underline{x}_{n+1}$  by integration of:

$$\frac{d\underline{x}_j}{dt} = \underline{\underline{C}}_j \underline{x}_j + \underline{\underline{d}}_x_j, \quad j = 1, \dots, C$$

2. Solve bubble point eqn. for

$$T_{i,n+1}, \underline{y}_{i,n+1} \quad i = 1, \dots, N$$

3. Solve Eqs. 14 and 15

$$\text{Estimate } \Delta h_i^L / \Delta t \text{ and } \Delta M_i / \Delta t \text{ at } t_n, \quad i = 1, \dots, N$$

$$\text{Calculate } \underline{\underline{L}}_{n+1}, \underline{V}_{n+1}$$

4. Compute  $\rho_{i,n+1}^L$

$$M_i = \rho_{i,n+1}^L A_i [H_{w_i} + \Delta_{w_{i,n+1}}] \\ \uparrow 1.41 \left( \frac{L_{i,n+1}}{\sqrt{g} \rho_{i,n+1}^L L_{w_i}} \right)^{2/3}$$

5. Let  $n \leftarrow n + 1$

Figure 3. Distefano algorithm.

#### Distefano Algorithm

Distefano (1968a) accompanied Eq. 8 with two other working equations. He combined the energy balance (Eq. 4) with the overall mass balance to give (ignoring side streams):

$$\frac{dh_i^L}{dt} = f_i^h = \frac{1}{M_i} [L_{i+1}(h_{i+1}^L - h_i^L) - V_i(h_i^v - h_i^L) + V_{i-1}(h_{i-1}^v - h_i^L) + F_i(h_i^F - h_i^L) + Q_i] \quad i = 1, \dots, N \quad (13)$$

The third set of ODE's are the overall mass balances:

$$\frac{dM_i}{dt} = f_i^M = L_{i+1} + V_{i-1} + F_i - L_i - V_i \quad i = 1, \dots, N \quad (2)$$

Values of  $\underline{x}_{n+1}$ ,  $\underline{\underline{L}}_{n+1}$ , and  $\underline{\underline{M}}_{n+1}$  could be computed by numerical integration. However,  $\underline{\underline{L}}_{n+1}$  and  $\underline{\underline{M}}_{n+1}$  are not independent of  $\underline{x}_{n+1}$ . Given  $\underline{x}_{n+1}$ ,  $\underline{T}_{n+1}$  can be computed by solution of Eq. 12, followed by  $\underline{\underline{L}}_{n+1}$ ,  $\rho_{n+1}^L$ , and  $\underline{\underline{M}}_{n+1}$  (assuming constant volume hold-up).

Distefano uses Eqs. 13 and 2, with approximations for the derivatives,  $dh_i^L/dt$  and  $dM_i/dt$ , to give  $\underline{\underline{V}}_{n+1}$  and  $\underline{\underline{L}}_{n+1}$ . Since these derivatives are not normally large, he recommends low-order finite-difference approximations:

$$\frac{\Delta h_i^L}{\Delta t} = \frac{1}{M_i} [L_{i+1}(h_{i+1}^L - h_i^L) - V_i(h_i^v - h_i^L) + V_{i-1}(h_{i-1}^v - h_i^L) + F_i(h_i^F - h_i^L) + Q_i] \quad (14)$$

and

$$\frac{\Delta M_i}{\Delta t} = L_{i+1} + V_{i-1} + F_i - L_i - V_i \quad (15)$$

but does not indicate his choice of approximations. His algorithm for integration of Eq. 8 and solution of Eqs. 12, 14 and 15 is summarized in Figure 3.

It is noteworthy that the GEAR integrator (Hindmarsh, 1974) can be used to approximate  $dh_i^L/dt$  and  $dM_i/dt$ . To show this, we must first review the GEAR integrator.

#### GEAR Integrator

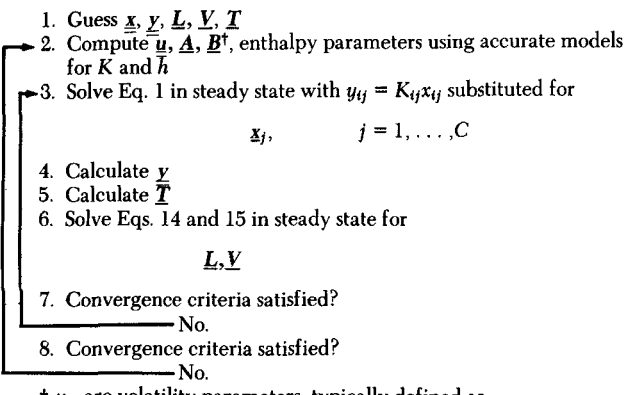
GEAR is a multistep algorithm for the integration of  $m$  stiff ODE's

$$\frac{dy}{dt} = f(y, t) \quad (16)$$

that uses backward difference formulas:

$$y_{n+1} = \sum_{l=0}^{r-1} \alpha_l y_{n-l} + h \beta_{-1} f(t_{n+1}, y_{n+1}) \quad (17)$$

where  $r$  is the order of accuracy of the formulas. The values of  $y$  at previous steps are computed using the Nordsieck array



†  $u_{ij}$  are volatility parameters, typically defined as

$$u_{ij} = \frac{K_{ij}}{K_i}$$

where

$$\ln \bar{K}_i = A_i - \frac{B_i}{T_i}$$

(a) Approximation to the Boston and Sullivan algorithm for solution of MESH equations in the steady-state

(b) Modified Boston and Sullivan algorithm.

Figure 4. Boston and coworkers algorithm using GEAR

$$\underline{z}_n = \left[ \underline{y}_n, h \dot{\underline{y}}_n, \frac{h^2}{2} \ddot{\underline{y}}_n, \dots, \frac{h^q}{q!} \underline{y}_n^{(q)} \right] \quad (18)$$

which has  $q$  columns, where  $r \leq q$ . The GEAR program updates the Nordsieck array during each time step, rather than store previous values of  $\underline{y}$  and carry-out interpolation when the step-size changes. "Near A-stability" or "stiff stability" is achieved by adjusting  $r$  and  $h$  simultaneously in an algorithm described by Hindmarsh (1974), where  $1 \leq r \leq 6$ . During each time step, the Newton-Raphson method is used to solve Eq. 17 for  $\underline{y}_{n+1}$ . Normally only one iteration is necessary and the Jacobian matrix is evaluated once every few time steps. A disadvantage of the GEAR algorithm is that the Nordsieck array requires storage for  $q = 6$  vectors having  $m$  elements, where  $m$  is the number of state variables.

#### Algorithm of Boston and Coworkers

The GEAR algorithm can be used for integration of Eq. 8 with Eq. 11 or Eqs. 13 and 2. But, since Eq. 17 must be solved for the state variables with the algebraic MESH equations, Boston and coworkers (1981) prefer to use their efficient RADFRAC program with modifications. RADFRAC solves the MESH equations in the steady-state using the Boston and Sullivan algorithm (1974).

Rather than present the details of this complex algorithm, Figure 4a gives an approximation that we have found works well. The  $K$ -values and enthalpies are evaluated accurately in the outer loop only. The MESH equations are solved in the inner loop using approximate models for  $K$ -values and enthalpies and holding  $u, A, B$  (defined in Figure 4a) and enthalpy parameters constant. In our experience, the computation time to solve the MESH equations in the inner loop is equivalent to that for one iteration of the outer loop.

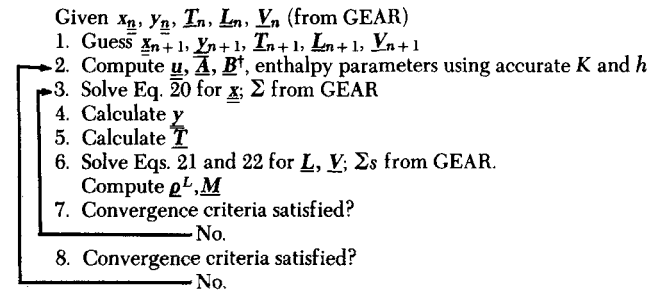
Step 3 solves the material balances for species  $j$  in the steady-state (Eq. 1) with  $y_{ij} = K_{ij} x_{ij}$  substituted:

$$\begin{aligned} \hat{f}_{ij} &= (1 - s_{i+1}^L) L_{i+1} x_{i+1,j} - (L_i + V_i K_{ij}) x_{ij} \\ &+ (1 - s_{i-1}^v) V_{i-1} K_{i-1,j} x_{i-1,j} + F_i z_{ij} = 0, \\ \hat{f}_j &= \hat{G}_j x_j + d_j \end{aligned} \quad (19)$$

For dynamic simulation, however, Eq. 8

$$\frac{d x_j}{dt} = f_j = \underline{G}_j x_j + \underline{d}_j, \quad j = 1, \dots, C \quad (8)$$

must be integrated from  $t_n$  to  $t_{n+1}$ . Note that  $\underline{G}_j$  and  $\hat{G}_j$  are tri-



Given  $\underline{x}_n, \underline{y}_n, \underline{T}_n, \underline{L}_n, \underline{V}_n$  (from GEAR)

1. Guess  $\underline{x}_{n+1}, \underline{y}_{n+1}, \underline{T}_{n+1}, \underline{L}_{n+1}, \underline{V}_{n+1}$

2. Compute  $\underline{u}, \underline{A}, \underline{B}$ , enthalpy parameters using accurate  $K$  and  $h$

3. Solve Eq. 20 for  $\underline{x}, \Sigma$  from GEAR

4. Calculate  $\underline{y}$

5. Calculate  $\underline{T}$

6. Solve Eqs. 21 and 22 for  $\underline{L}, \underline{V}, \Sigma$  from GEAR.

Compute  $\rho^L, M$

7. Convergence criteria satisfied?

No.

8. Convergence criteria satisfied?

No.

Given  $\underline{x}_n, \underline{y}_n, \underline{T}_n, \underline{L}_n, \underline{V}_n$  (from GEAR)

1. Guess  $\underline{x}_{n+1}, \underline{y}_{n+1}, \underline{T}_{n+1}, \underline{L}_{n+1}, \underline{V}_{n+1}$

2. Compute  $\underline{u}, \underline{A}, \underline{B}$ , enthalpy parameters using accurate  $K$  and  $h$

3. Solve Eq. 20 for  $\underline{x}, \Sigma$  from GEAR

4. Calculate  $\underline{y}$

5. Calculate  $\underline{T}$

6. Solve Eqs. 21 and 22 for  $\underline{L}, \underline{V}, \Sigma$  from GEAR.

Compute  $\rho^L, M$

7. Convergence criteria satisfied?

No.

8. Convergence criteria satisfied?

No.

diagonal matrices with similar elements;  $\underline{G}_j$  are a function of  $\underline{M}$ .

Boston and coworkers (1981) use the GEAR algorithm to integrate Eq. 8 from  $t_n$  to  $t_{n+1}$ . The resulting nonlinear algebraic equations:

$$\underline{x}_{j,n+1} = \sum_{l=1}^{r-1} \alpha_l \underline{x}_{j,n-l+1} + h \beta_{-1} f_j \{ \underline{x}_{j,n+1}, t_{n+1} \} \quad (20)$$

differ slightly from Eq. 19. Hence, the Boston and Sullivan algorithm is modified to solve Eq. 20 rather than Eq. 19 in Step 3. The GEAR subroutine STIFF is also modified to transfer the summation term in Eq. 20

$$\sum_{l=1}^{r-1} \alpha_l \underline{x}_{j,n-l+1}$$

and the step size,  $h$ , to the modified Boston and Sullivan algorithm, which solves the MESH equations for  $\underline{x}_{j,n+1}$  (and  $\underline{y}_{j,n+1}, \underline{T}_{n+1}, \underline{V}_{n+1}$  and  $\underline{L}_{n+1}$ ) and returns to the GEAR integrator, as illustrated in Figure 4b. Note that the GEAR integrator also integrates Eqs. 13 and 2 and the resulting equations:

$$h_{i,n+1}^L = \sum_{l=1}^{r-1} \alpha_l h_{i,n-l+1}^L + h \beta_{-1} f_i^h \{ h_{i,n+1}^L, t_{n+1} \} \quad (21)$$

$$M_{i,n+1} = \sum_{l=1}^{r-1} \alpha_l M_{i,n-l+1} + h \beta_{-1} f_i^M \{ M_{i,n+1}, t_{n+1} \} \quad (22)$$

differ from those in the steady state:

$$\begin{aligned} \hat{f}_i^h &= L_{i+1} h_{i+1}^L + V_{i-1} h_{i-1}^v + F_i h_i^F + Q_i = 0 \quad (23) \\ \hat{f}_i^M &= L_{i+1} + V_{i-1} + F_i - L_i - V_i = 0 \end{aligned}$$

where  $f_i^h = (\hat{f}_i^h - h_i \hat{f}_i^M) / M_i$  and  $f_i^M = \hat{f}_i^M$ . Hence, the Boston and Sullivan algorithm is modified to solve Eqs. 21 and 22 for  $\underline{V}$  and  $\underline{L}$  in Step 6, rather than Eqs. 23 and 24. The GEAR subroutine STIFF transfers the summations and  $h_{i,n+1}^L$  and  $M_{i,n+1}$  are computed using  $\underline{x}_{i,n+1}$  and  $T_{i,n+1}$ .

#### Other Algorithms

Gallun and Holland (1980) and Sourisseau and Doherty (1980) also use the GEAR integrator. Both solve the MESH equations with the pressure head computed for each tray, although Sourisseau and Doherty consider binary systems only. Gallun and Holland indicate

that the GEAR integrator must be modified to solve the difference equations and the other nonlinear algebraic equations. However, neither paper presents an algorithm to accomplish this.

### ASIRK Integrator

As mentioned previously, our adaptive semi-implicit Runge-Kutta (ASIRK) integrator (Prokopakis and Seider, 1981b) has been observed to take larger time steps than the GEAR integrator to achieve comparable accuracy. Normally, a penalty is paid for additional Jacobian evaluations, but ASIRK was developed given the Ballard and Brosilow observation that the elements of the Jacobian for the MESH equations are computed during evaluation of the functions,  $f_j$ ,  $j = 1, \dots, C$ , since

$$\underline{J}_j \simeq \underline{G}_j \quad j = 1, \dots, C \quad (25)$$

This is a fine approximation because the elements of  $\underline{G}_j$  do not vary appreciably with  $\underline{x}_j$  across a time step; in support of this, Kim and Friedly (1974) demonstrate that the response times for  $\underline{x}$  are significantly greater than for  $\underline{L}$ . Furthermore, the approximation is reasonable for highly nonideal solutions. Before describing the algorithm for integration of the MESH equations, we briefly review the features of the ASIRK integrator.

The integration formula is:

$$\underline{y}_{n+1} = \underline{y}_n + w_1 \underline{k}_1 + w_2 \underline{k}_2 \quad (26)$$

where

$$[\underline{I} - ha \underline{J} \{ \underline{y}_n \}] \underline{k}_1 = h \underline{f} \{ \underline{y}_n \} \quad (27)$$

$$[\underline{I} - ha \underline{J} \{ \underline{y}_n \}] \underline{k}_2 = h \underline{f} \{ \underline{y}_n + b \underline{k}_1 \} \quad (28)$$

Although the method is derived to give second-order accuracy, the coefficients  $w_1$ ,  $w_2$ ,  $a$ , and  $b$  are adjusted to give an exact solution to:

$$\frac{dy_s}{dt} = \bar{\lambda}_s y_s \quad (29)$$

over the last time step, where  $y_s$  is the variable having the largest fractional rate of change; that is, the pseudo-eigenvalue,  $\bar{\lambda}_s$ , is estimated using values of  $y_s$  over the last time step. The step size,  $h$ , is projected using values of  $y_s$  over two previous time steps and the product  $h\bar{\lambda}_s$  is used to adjust  $\gamma_\infty$  (characteristic root of Eqs. 26-28

as  $h|\lambda| \rightarrow \infty$ ) and, in turn,  $w_1$ ,  $w_2$ ,  $a$  and  $b$  for integration over the next step. This algorithm gives much better than second-order accuracy in tracking the variable having the largest fractional rate of change, as well as the remaining variables. Unfortunately, the methods of estimating  $\bar{\lambda}_s$ , projecting  $h$ , and adjusting  $\gamma_\infty$  cannot be summarized in a few sentences. The reader should refer to our paper (Prokopakis and Seider, 1981b) for the details.

Since ASIRK is a single-step method, it requires less storage ( $\underline{y}_n$  and  $y_{s,n-1}$ ) than the GEAR method (Nordsieck array, six columns). Also, ASIRK is A-stable, whereas the family of backward difference formulas in the GEAR method are just stiffly stable.

### ASIRK METHOD FOR INTEGRATION OF THE MESH ODE'S

When integrating with the ASIRK method, the system is decoupled; that is, each of  $C$  sets of  $N$  ODE's is integrated independently:

$$\begin{aligned} \underline{x}_{j,n+1} &= \underline{x}_{j,n} + w_1 \underline{k}_{1,j} + w_2 \underline{k}_{2,j} \quad j = 1, \dots, C \\ \underline{k}_{1,j} &= [\underline{I} - ah \underline{G}_j]^{-1} h \underline{f}_j \{ \underline{x}_{j,n} \} \\ \underline{k}_{2,j} &= [\underline{I} - ah \underline{G}_j]^{-1} h \underline{f}_j \{ \underline{x}_{j,n} + b \underline{k}_{1,j} \} \end{aligned} \quad (30)$$

Note that  $\underline{J}_j$  has been replaced by  $\underline{G}_j$ , the elements of which are computed when evaluating  $\underline{f}_j$  (Eq. 8). We integrate Eq. 8 with finite-difference approximations for  $dh_i^L/dt$  and  $dM_i/dt$  in Eqs. 13 and 2, as recommended by Distefano. We use second-order backward differences, which require storage of  $\underline{h}^L$  and  $\underline{M}$  over the two previous time steps. The algorithm is shown in Figure 5a.

To estimate  $\Delta h_i^L/\Delta t$  and  $\Delta M_i/\Delta t$  initially, we assume the tower operates at steady-state prior to a disturbance. If the flow rate of a feed stream changes by  $\Delta F_i$  at  $t = 0$ ,

$$\left( \frac{\Delta M_i}{\Delta t} \right)_{t=0} \simeq \Delta F_i$$

and

$$\left( \frac{\Delta h_i^L}{\Delta t} \right)_{t=0} \simeq \frac{1}{M_i} \left[ (\Delta F_i) h_i^F - h_i^L \left( \frac{\Delta M_i}{\Delta t} \right)_{t=0} \right]$$

For the second and subsequent steps first-order backward differ-

Given  $\underline{x}_n$ ,  $\underline{y}_n$ ,  $\underline{T}_n$ ,  $\underline{L}_n$ ,  $\underline{V}_n$

1. Estimate  $\Delta h_i^L/\Delta t$  and  $\Delta M_i/\Delta t$  at  $t_n$ ,  $i = 1, \dots, N$
2. Calculate  $\underline{k}_{1,j}$

$$[\underline{I} - ha \underline{G}_j \{ \underline{x}_{j,n} \}] \underline{k}_{1,j} = h [\underline{G}_j \{ \underline{x}_{j,n} \} \underline{x}_{j,n} + \underline{d}_{x,j}] \quad j = 1, \dots, C$$

3. At  $\underline{x}_{j,n} + b \underline{k}_{1,j}$ , compute

$$\begin{aligned} \underline{T}, \underline{y} &\text{ using Eq. 31} \\ \underline{L}, \underline{V} &\text{ using Eqs. 14 and 15} \\ \underline{\rho}^L, \underline{M} & \end{aligned}$$

4. Calculate  $\underline{k}_{2,j}$

$$[\underline{I} - ha \underline{G}_j \{ \underline{x}_{j,n} \}] \underline{k}_{2,j} = h [\underline{G}_j \{ \underline{x}_{j,n} + b \underline{k}_{1,j} \} (\underline{x}_{j,n} + b \underline{k}_{1,j}) + \underline{d}_{x,j}] \quad j = 1, \dots, C$$

5. Compute

$$\underline{x}_{j,n+1} = \underline{x}_{j,n} + w_1 \underline{k}_{1,j} + w_2 \underline{k}_{2,j} \quad j = 1, \dots, C$$

6. At  $t_{n+1}$ , compute

$$\begin{aligned} \underline{T}_{n+1}, \underline{y}_{n+1} &\text{ using Eq. 31} \\ \underline{L}_{n+1}, \underline{V}_{n+1} &\text{ using Eqs. 14 and 15} \\ \underline{\rho}^L_{n+1}, \underline{M}_{n+1} & \end{aligned}$$

7. Let  $n \leftarrow n + 1$

(a) Distefano algorithm

Given  $\underline{x}_n$ ,  $\underline{y}_n$ ,  $\underline{T}_n$ ,  $\underline{L}_n$ ,  $\underline{V}_n$

1. Calculate  $\underline{k}_{1,j}$

$$[\underline{I} - ha \underline{G}_j \{ \underline{x}_{j,n} \}] \underline{k}_{1,j} = h [\underline{G}_j \{ \underline{x}_{j,n} \} \underline{x}_{j,n} + \underline{d}_{x,j}] \quad j = 1, \dots, C$$

$$[\underline{I} - ha \underline{J}_L \{ \underline{L}_n \}] \underline{k}_{1,L} = h [\underline{J}_L \{ \underline{L}_n \} \underline{L}_n + \underline{d}_{L,n}]$$

2. At  $\underline{x}_{j,n} + b \underline{k}_{1,j}$  and  $\underline{L}_n + b \underline{k}_{1,L}$ , compute

$$\begin{aligned} \underline{T}, \underline{y} &\text{ using Eq. 31} \\ \underline{V} &\equiv \underline{C}^{-1} [\underline{d}_E - \underline{B}(\underline{L}_n + b \underline{k}_{1,L})] \end{aligned}$$

3. Calculate  $\underline{k}_{2,j}$

$$[\underline{I} - ha \underline{G}_j \{ \underline{x}_{j,n} \}] \underline{k}_{2,j} = h [\underline{G}_j \{ \underline{x}_{j,n} + b \underline{k}_{1,j} \} (\underline{x}_{j,n} + b \underline{k}_{1,j}) + \underline{d}_{x,j}]$$

$$[\underline{I} - ha \underline{J}_L \{ \underline{L}_n \}] \underline{k}_{2,L} = h [\underline{J}_L \{ \underline{L}_n + b \underline{k}_{1,L} \} (\underline{L}_n + b \underline{k}_{1,L}) + \underline{d}_L]$$

4. Compute

$$\begin{aligned} \underline{x}_{j,n+1} &= \underline{x}_{j,n} + w_1 \underline{k}_{1,j} + w_2 \underline{k}_{2,j} \quad j = 1, \dots, C \\ \underline{L}_{n+1} &= \underline{L}_n + w_1 \underline{k}_{1,L} + w_2 \underline{k}_{2,L} \end{aligned}$$

5. At  $t_{n+1}$ , compute

$$\begin{aligned} \underline{T}_{n+1}, \underline{y}_{n+1} &\text{ using Eq. 31} \\ \underline{V}_{n+1} &\equiv \underline{C}^{-1} [\underline{d}_E - \underline{B}(\underline{L}_{n+1})] \end{aligned}$$

6. Let  $n \leftarrow n + 1$

(b) Ballard and Brosilow algorithm.

Figure 5. Distillation algorithms using ASIRK

ences are used with  $h_i^L$  and  $M_i$  values at the beginning and end of the last time step. Other disturbances are treated similarly.

To locate the bubble point temperature,  $T_i$ , and  $y_i$ , we rewrite Eq. 12, as recommended by Prausnitz and coworkers (1980):

$$f\{1/T_i\} = \ln \left\{ \sum_{j=1}^C K_{ij} x_{ij} \right\} = 0 \quad (31)$$

because the  $K$ -values,  $K_{ij}$ , vary with  $\exp\{1/T_i\}$ , and, hence,  $f$  is nearly a linear function of  $1/T_i$ . We have found that the Newton-Raphson method works well to solve Eq. 31, requiring no more than two iterations after the initial profile is computed for the azeotropic distillation towers in this paper (relative error tolerance = 0.001).

Ballard and Brosilow add  $N$  ODE's in Eq. 11 and show that

$$\underline{M}_L^{-1}(\underline{D} - \underline{E}\underline{C}^{-1}\underline{B}) \simeq \underline{M}_L^{-1}\underline{D},$$

except for unusually large time steps, and recommend taking

$$\underline{J}_L \simeq \underline{M}_L^{-1}\underline{D} \quad (32)$$

to avoid numerical differentiation. This set of  $N$  ODE's is also integrated independently with the ASIRK method and a revised algorithm is given in Figure 5b.

### Multicomponent Systems

Often the mole fractions for one or more of the species do not change appreciably and it is possible to avoid re-evaluation of  $[\underline{I} - ah\underline{J}_j]^{-1}$  or even integration for a subset of the ODE's. We have found the pseudo-eigenvalue,  $\bar{\lambda}_{sj}$ , is a good measure of the rate of change and use it to indicate when these steps are unnecessary.

For each set of  $N$  ODE's, prior to each integration time step, we estimate the pseudo-eigenvalue  $\bar{\lambda}_{sj}$ ,  $j = 1, \dots, C$  and  $\bar{\lambda}_{sL}$  ( $L = C + 1$ ), and take the largest,  $\bar{\lambda}_{s,\max}$ , as the pseudo-eigenvalue for the entire system. Then, each set of ODE's is classified in one of three categories:

(1) Negligible rate of change when

$$|\bar{\lambda}_{sj}/\bar{\lambda}_{s,\max}| < \kappa \quad j = 1, \dots, C + 1 \quad (33)$$

where  $\kappa = 10^{-4}$  has produced good results in our studies. Equations in this category are not integrated.

(2) Moderate rate of change when

$$\kappa < |\bar{\lambda}_{sj}/\bar{\lambda}_{s,\max}| < \theta \quad j = 1, \dots, C + 1 \quad (34)$$

where  $\theta = 0.5$  has also produced good results. Equations in this category are integrated, but without recomputing  $[\underline{I} - ah\underline{J}_j]^{-1}$ .

(3) Rapid rate of change when

$$\theta < |\bar{\lambda}_{sj}/\bar{\lambda}_{s,\max}| \quad j = 1, \dots, C + 1 \quad (35)$$

Equations in this category are integrated with new  $[\underline{I} - ah\underline{J}_j]^{-1}$ . Usually these have flow rates as output variables. Clearly the values for  $\kappa$  and  $\theta$  are arbitrary and may need to be adjusted to improve performance for a particular system.

Next we consider the mechanics of integration for sets of ODE's classified as having rapid or moderate rates of change. We let  $y_s$  be the variable with the largest fractional rate of change during the last time-step, corresponding to  $\bar{\lambda}_{s,\max}$ . Following the ASIRK algorithm,  $h_{n+1}$  is estimated using  $y_{s,n}$ ,  $y_{s,n-1}$ , and  $y_{s,n-2}$ . Then  $\gamma_\infty$  is computed for  $h_{n+1}\bar{\lambda}_{s,\max}$  and the parameters  $a$ ,  $b$ ,  $w_1$ , and  $w_2$  are computed, prior to integrating the set of  $N$  ODE's with  $y_s$  as an output variable. For other sets of ODE's having rapid rate of change, we recompute  $[\underline{I} - ah\underline{J}_j]^{-1}$ .

For sets with moderate rate of change, to avoid recomputing  $[\underline{I} - ah\underline{J}_j]^{-1}$ , we assume that  $\underline{J}_j$  does not change between iterations and set

$$a_{n+1} = \frac{a_n h_n}{h_{n+1}} \quad (36)$$

Then  $\gamma_\infty$  is computed and the remaining parameters,  $b$ ,  $w_1$ ,  $w_2$ , are computed. Here  $\gamma_\infty$  is not adjusted to give high accuracy, but the rate of change is moderate and the step size is less than necessary for these sets of ODEs. After five time steps, we check whether

$$\|\underline{J}_{j,n+1} - \underline{J}_{j,n}\| \leq 0.1$$

If not,  $[\underline{I} - ah\underline{J}_j]^{-1}$  is recomputed.

### AZEOTROPIC DISTILLATION

In previous work (Prokopakis and Seider, 1983), we used a nonlinear programming algorithm to obtain feasible operating conditions for the azeotropic distillation configuration in Figure 6a to dehydrate alcohol. The boil-up rate, fractional recovery of product, and bottoms purities of entrainer and by-product are adjusted to locate an overhead vapor stream that condenses into two liquid phases, but is in equilibrium with a single liquid phase on the top tray. Our results show the extreme sensitivity of the overhead vapor composition and the steep concentration and temperature fronts to small changes in these variables. Furthermore, they show three regimes of operation, which were simultaneously reported by Magnusson and coworkers (1979), who found an instance of instability for one of the regimes. These observations suggested that dynamic simulation studies might uncover unusual

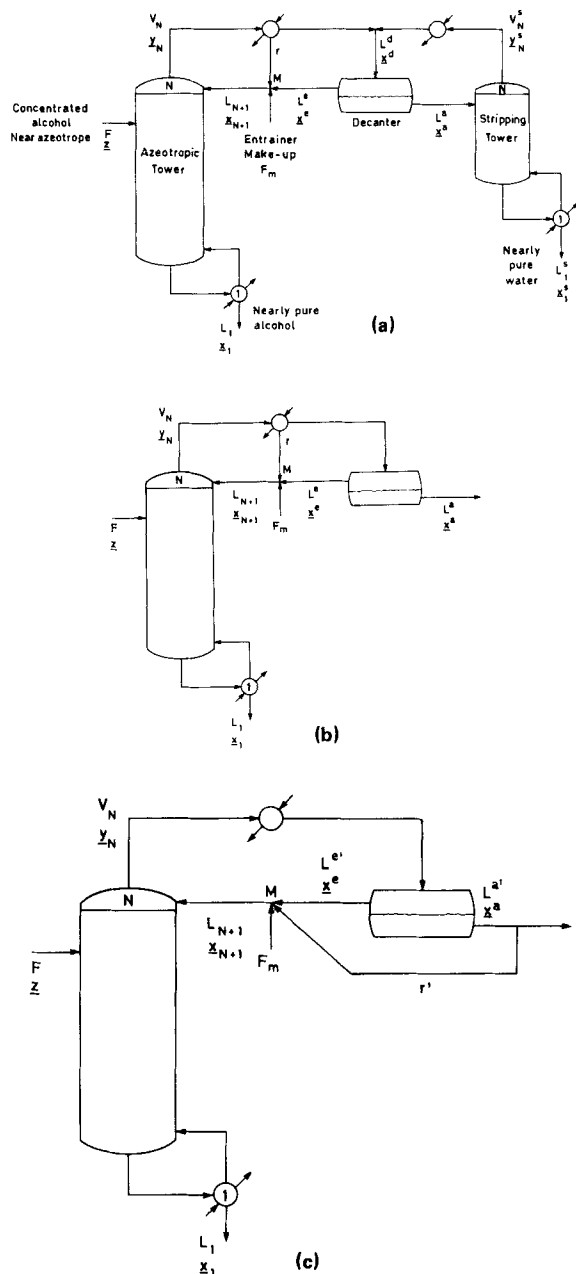


Figure 6. Configurations for dehydration of alcohol.

responses to disturbances as well as support the observations of Magnussen and coworkers.

Our steady-state results show that the aqueous phase leaving the decanter is small compared with the entrainer phase, and with water removed in the stripping tower, the flow rate of the vapor overhead stream,  $V_N^s$ , is small compared to  $V_N(1-r)$ . Hence, to study dynamic responses, it should be possible to exclude the stripping tower, as illustrated in Figure 6b, without incurring significant errors. Figure 6c gives a similar configuration, commonly found in industry, and it can be shown that  $r = r'$  for given  $V_1, L_1, \underline{x}_1, T^d$ , and  $F_m$ . The latter configuration was simulated in these studies and, hence, our nonlinear programming problem (Prokopakis and Seider, 1983) was modified to locate steady-state conditions. The modifications are summarized in Appendix A.

The model for dynamic simulation of the azeotropic tower has been presented, as well as algorithms to integrate the MESH ODE's. In this work, the reboiler, Tray 1, is assigned a large holdup at constant volume.

## Decanter

The dynamics of the decanter are modeled separately with the following assumptions:

- (1) The holdup is large and constant in volume.
- (2) The temperature is constant (which requires the heat duty of the condenser to vary).
- (3) The two liquid phases leave the decanter at equilibrium.
- (4) The two liquid phases are perfectly mixed.

These lead to the following equations, beginning with the material balances for species  $j$

$$\frac{d}{dt}(M^{d'}x_j^d) = V_N y_{N,j} - L^{e'}x_j^e - L^{a'}x_j^a \quad j = 1, \dots, C \quad (37)$$

where

$$M^{d'} = G^d \rho \{ \underline{x}^d, T^d \} \quad (38)$$

and  $G^d$  is the volume of hold-up in the decanter. The overall mass balance is:

$$\frac{dM^{d'}}{dt} = V_N - L^{e'} - L^{a'} \quad (39)$$

and the equations that relate the composition in the two liquid phases at equilibrium are:

$$x_j^e = K_j^d \{ \underline{x}^e, \underline{x}^a, T^d \} x_j^a \quad j = 1, \dots, C \quad (40)$$

The derivative of Eq. 37 is expanded and Eqn. 39 substituted. Since

$$x_j^d (L^{e'} + L^{a'}) = x_j^e L^{e'} + x_j^a L^{a'},$$

we have:

$$\frac{dx_j^d}{dt} = \frac{V_N}{M^{d'}} (y_{N,j} - x_j^d) \quad (41)$$

During each time step, Eq. 41 is integrated to give  $\underline{x}_{n+1}^d$ , given  $V_N$  and  $\underline{y}_N$  from integration of the MESH ODE's for the azeotropic tower. Then, the feed to the decanter is split into two liquid phases, giving  $\underline{x}^e$ ,  $\underline{x}^a$  and  $\beta = L^{e'}/(L^{e'} + L^{a'})$ . Assumption (1) gives:

$$\frac{V_N}{\rho \{ \underline{y}_N, T^d \}} = \frac{L^{e'} + L^{a'}}{\rho \{ \underline{x}^d, T^d \}},$$

and with  $\beta$  computed,  $L^{e'}$  and  $L^{a'}$  are computed. Furthermore, by assumption (3),

$$\beta = \frac{L^{e'}}{L^{e'} + L^{a'}} = \frac{M^{e'}}{M^{e'} + M^{a'}}$$

## RESULTS

Two systems were used to study the open loop response of azeotropic distillation towers: (1) dehydration of ethanol with

benzene, and (2) dehydration of isopropanol with cyclohexane. The equations for estimating the thermophysical properties and the sources of parameters are summarized in Appendix B.

### Ethanol Dehydration with Benzene

Calculations were performed for a 27-tray tower (including the reboiler) to dehydrate a stream containing 89 mol/min of ethanol and 11 mol/min of water. This saturated liquid feed is introduced on Tray 23. The pressure increases from 1.013 bar at the top to 1.216 bar in the reboiler, with uniform pressure increase from tray to tray.

Feasible specifications were obtained using our nonlinear programming algorithm (Prokopakis and Seider, 1983), as modified for the configuration in Figure 6c. (See Appendix A.) We solved  $P_1$  with  $V_1^L = 250$  mol/min,  $R_{alc}^L = 0.9$ ,  $R_{alc}^U = 1.0$ ,  $x_{1,ent}^U = x_{1,wat}^U = 5 \times 10^{-4}$ , and  $T_{N+1} = 298$  K, and obtained  $V_1 = 439.5$  mol/min,  $R_{alc} = 0.905$ ,  $x_{1,ent} = 2.433 \times 10^{-4}$ ,  $x_{1,wat} = 2.910 \times 10^{-4}$ , and

$$Q_1 = 1.787 \times 10^7 \text{ J/min}$$

$$V_N = 487.1 \text{ mol/min}, \quad \underline{y}_N = [0.2578 \quad 0.5529 \quad 0.1893]^T$$

$$L_{N+1} = 467.7 \text{ mol/min}, \quad \underline{x}_{N+1} = [0.2504 \quad 0.5759 \quad 0.1737]^T$$

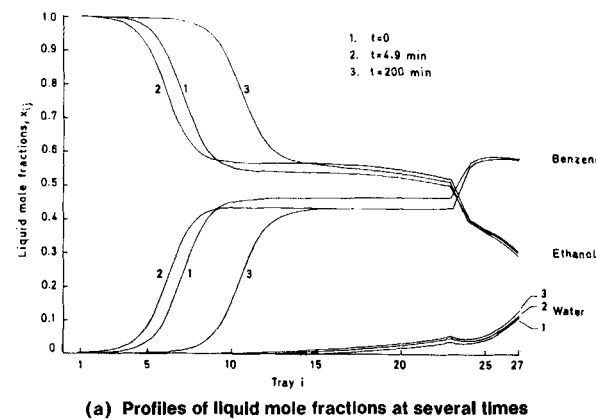
$$F_m = 1.965 \text{ mol/min}$$

$$r = 0.8347, \quad R = 5.05$$

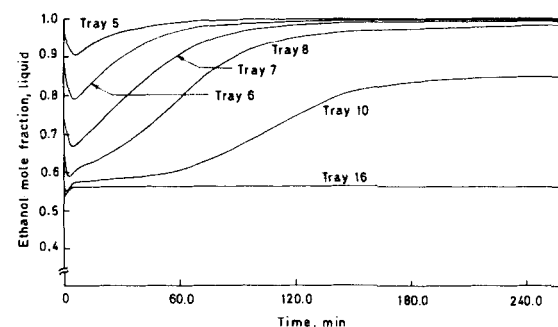
The profiles of liquid mole fractions are shown in Figure 7a at  $t = 0$ .

The dynamic simulation studies tracked disturbances about this steady state for a tower with  $A_t = 0.23 \text{ m}^2$ , to give a linear vapor velocity of approximately 1 m/s, and  $H_{w_t} = 0.0254 \text{ m}$ . The crest height,  $\Delta_{w_t}$ , was assumed equal to  $0.2 H_{w_t}$ . The reboiler and decanter holdups were 1 m<sup>3</sup>.

Typically, the feed flow rate is disturbed, causing a shift in the concentration and temperature profiles, which can be countered by adjusting the decanter bypass fraction,  $r$ , the reboiler heat duty,  $Q_1$ , the condenser heat duty,  $Q^c$ , or the entrainer make-up flow



(a) Profiles of liquid mole fractions at several times



(b) Alcohol mole fractions on several trays.

Figure 7. Responses after a 30 percent increase in the feed flowrate

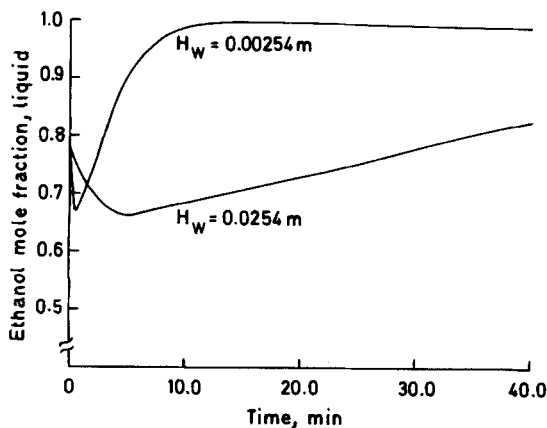


Figure 8. Effect of holdup. Ethanol mole fraction on Tray 7 after a 30 percent increase in the feed flowrate.

rate,  $F_m$ , or some combination of these. However, in our simulations,  $T^d$  is fixed at 298 K because activity coefficients cannot be computed accurately at other temperatures; hence,  $Q^c$  is not a control variable. Furthermore, the entrainer make-up stream is too small for control action. Hence, our studies were restricted to the open-loop responses for disturbances in the feed flow rate,  $r$ , and  $Q_1$ .

First, we increased the feed flow rate by 30% and observed the movement of concentration fronts in Figure 7a. After a small shift downward, the fronts shift upward. This upward shift is anticipated as the additional feed increases the water/entrainer ratio entering the tower, displacing the entrainer upward. This effect is further illustrated in Figure 7b, where the mole fraction of alcohol is tracked on several trays. Initially, the front passes through Trays 4–10. After a shift downward, it moves upward to pass through Trays 7–14 after 200 minutes. The temporary shift downward is due to "wash-out" with the feed liquid and decreases in duration with smaller hold-up, Figure 8. Initially, the mole fractions of ethanol and water increase on the feed tray and this disturbance is transmitted to the lower trays; *viz.*, wash-out. The separation becomes less effective as the alcohol concentration in the bottoms decreases slightly, first replaced by benzene. In time, the alcohol concentration decreases further with a build-up of water. Such an "inverse response" was unexpected, but is explained by the wash-out action. Upon closer examination, a similar effect is observed in the dynamic studies of Peiser and Grover (1962).

Next, we decreased the feed flow rate and observed the opposite effects, as illustrated in Figure 9 for a 10% decrease.

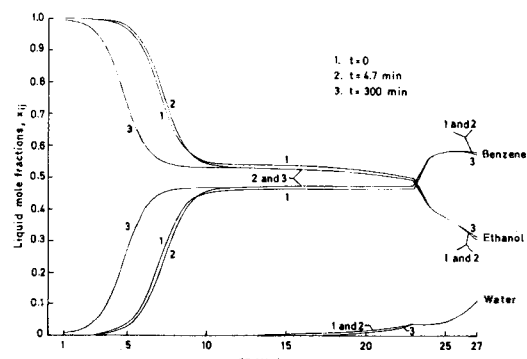
Similarly, we varied the composition of the binary feed stream. As expected, since additional water increases the water/entrainer ratio entering the tower, after a small shift downward due to wash-out, the fronts are displaced upward. The opposite effects were also observed.

Then, we varied the decanter bypass fraction. Additional bypass increases the water/entrainer ratio entering the tower. As above, after a small shift downward due to wash-out with the liquid reflux, the fronts are displaced upward, and the opposite effects are observed.

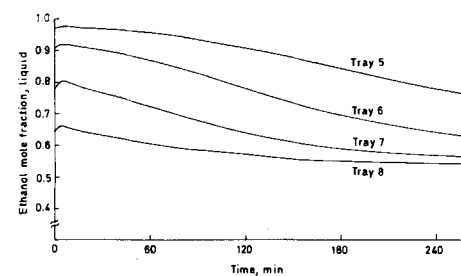
Finally, we varied the reboiler heat duty. For a given water/entrainer ratio entering the tower, additional boil-up lowers the ratio necessary for entrainer to penetrate into the stripping section. Excess entrainer shifts the fronts downward, after a small shift upward due to the step change in the boil-up. The opposite effects were also observed.

Results for step changes in the feed composition, the decanter bypass fraction, and the reboiler heat duty are not illustrated because they are qualitatively identical with those in Figures 7–9.

Control studies are beyond the scope of this work. However, to demonstrate the controllability of the azeotropic tower, we accompanied a 30% increase in feed flow rate with adjustments in the decanter bypass fraction and the reboiler heat duty to counter



(a) Profiles of liquid mole fractions at several times



(b) Alcohol mole fractions on several trays.

Figure 9. Responses after a 10 percent decrease in the feed

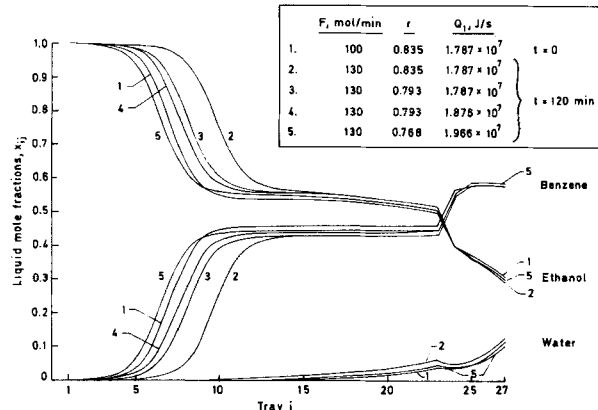


Figure 10. Profiles of liquid mole fractions two hours after four combinations of disturbances. Curves 1 give the initial steady-state profiles.

the shifts in the concentration and temperature fronts. The results are shown in Figure 10. Curve 1 shows the initial concentration profiles and Curve 2 shows the displacement, of approximately three trays, two hours after a 30% increase in the feed flow rate. For Curve 3, a 5% decrease in the decanter bypass fraction accompanied the increase in the feed flow rate, reducing the displacement to approximately one tray. For Curve 4, a 5% increase in the reboiler heat duty accompanied these changes, further reducing the displacement to approximately one-half tray. Finally, for Curve 5, an 8% decrease in  $r$  and a 10% increase in  $Q_1$  shift the fronts downward by approximately one-half tray.

Next, we introduced a larger disturbance in the feed flow rate to effect a shift in the regime of operation. The feed flow rate was increased by 60% and the results are shown in Figure 11. Only 3.5 minutes after the disturbance, the concentration fronts shift approximately two trays downward. Then, they gradually shift upward. After 17 hours the fronts are located between Trays 16 and 20 and the profiles resemble the second steady-state of Magnusson and coworkers (1979) (with appreciable water throughout and entrainer on the upper trays of the stripping section), which they report to be unstable. These results support this observation as the

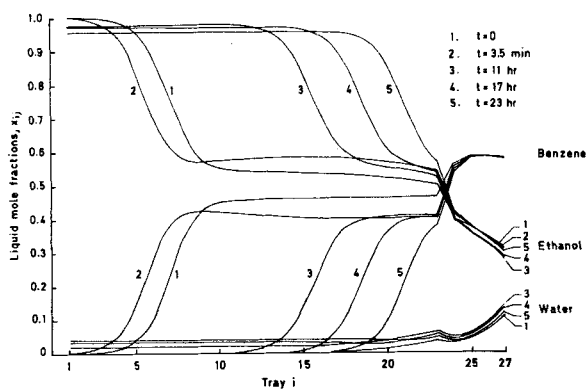


Figure 11. Profiles of liquid mole fractions at several times after a 60 percent increase in the feed flowrate.

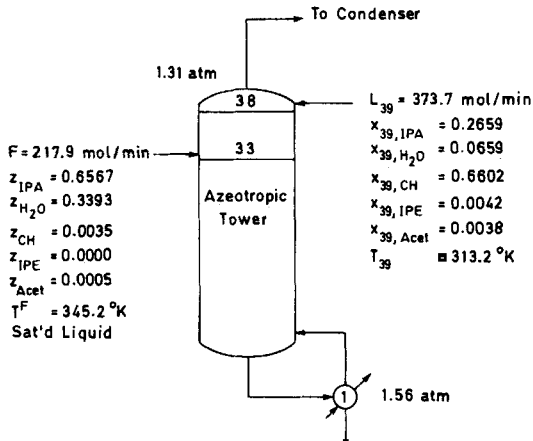


Figure 12. Dehydration of isopropanol with cyclohexane. Conditions typical of Union Carbide tower (Baldwin, 1979).

profiles drift through this regime and reach the third regime (Prokopakis and Seider, 1983) (with appreciable water, but no entrainer throughout the stripping section) after 23 hours.

Calculations for ethanol dehydration were performed using the Distefano algorithm with the ASIRK integrator (Figure 5a). A FORTRAN program was implemented on the UNIVAC 1100/61H computer and arithmetic operations were in single precision. Fifty-nine steps and 65 CPU seconds were required for 300 minutes of operation time after the feed was increased by 30%. The eigenvalues at  $t = 0$  were calculated and  $|\lambda|_{\max}$  was found to be 32; that is, the explicit Euler's method would require around 5,000 steps (assuming that  $|\lambda|_{\max}$  does not increase) for the integration from  $t = 0$  to  $t = 300$  min and an estimated 2,100 CPU seconds of the UNIVAC 1100 computer. This justifies the use of the stiff integrator. 280 CPU seconds were required to integrate the system from  $t = 0$  to  $t = 23$  h after the feed rate was increased by 60%. In the latter case, large time steps were taken as the system drifted slowly from one regime of operation to another.

The relative error tolerance for the ASIRK integrator was 0.1 and much smaller errors were obtained because error estimates of the imbedded pair in the ASIRK integrator are high. Several integrations were performed with a relative error tolerance of 0.01 for an hour of simulation time. The results agreed to four significant figures, except for mole fractions less than  $10^{-4}$ , where two figures were in agreement.

#### Dehydration of Isopropanol with Cyclohexane

Figure 12 shows a schematic of a 38-tray tower for dehydration of isopropanol with cyclohexane. The operating conditions are typical of a Union Carbide tower as provided by J. Baldwin in 1979.

In this section, we present the results of studies in which the re-

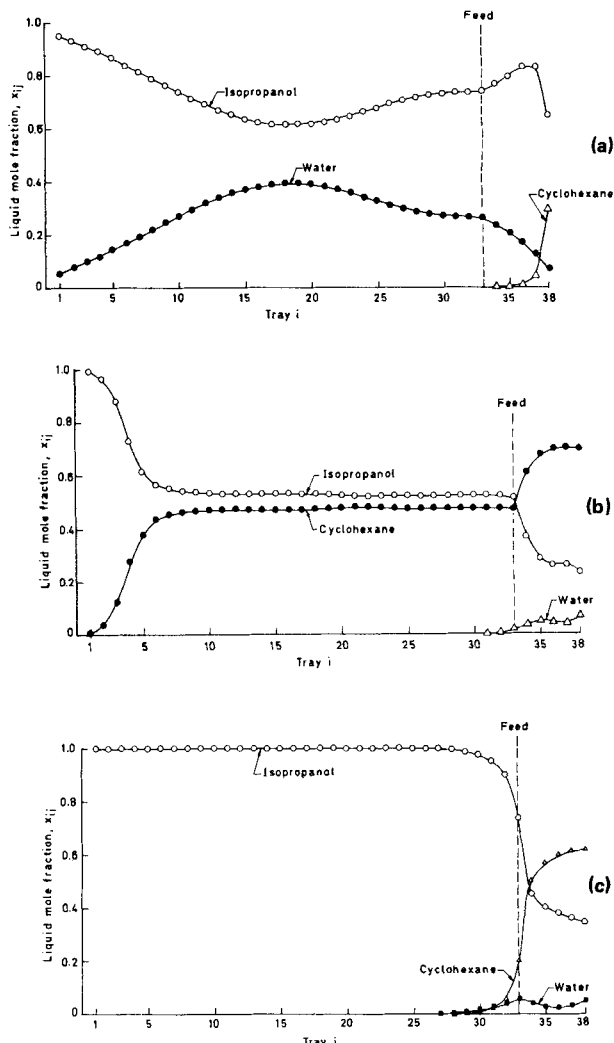


Figure 13. Profiles of liquid mole fraction.

flux was held fixed and the decanter disregarded. Furthermore, the reboiler hold-up was that of a typical tray and, hence, the degree of stiffness was reduced.

Initially, all trays were loaded with the feed mixture. The boil-up ratio was set to 5 and the concentration profiles in Figure 13a approached. However, the profiles drifted through this regime until the regime in Figure 13c was reached. Prokopakis and coworkers (1981a) computed a steady state similar to that in Figure 13a and these results imply that this steady state is unstable.

To obtain the profiles in Figure 13b, the conditions of Figure 13a were the initial conditions. The boil-up ratio was decreased to 3 and 100 mol of entrainer was added to the reboiler.

The Ballard and Brosilow algorithm with the ASIRK integrator (Figure 5b) was used to integrate  $(C + 1)N = (5 + 1)38 = 228$  ODE's. Using the classifications for multicomponent systems, for most time steps, only  $(2 + 1)38 + 3 \times 6 = 132$  ODE's were integrated. Note that isopropylether and acetone, and cyclohexane or water, do not concentrate in the stripping section. Yet, they have a moderate rate of change in the rectifying section. Hence, their ODE's in the rectifying section are integrated, but not those in the stripping section. Greater savings can be expected for systems with more chemical species.

#### Comparison with Other Algorithms

Unfortunately, the BATCHFRAC program by Boston and coworkers (1981) was unavailable and we have not implemented this algorithm. Hence, we are unable to compare its efficiency and reliability with our algorithms.

Tests of the Ballard and Brosilow integrator and the ASIRK in-

egrator for two and three ODE's, show the latter to be more efficient (Prokopakis and Seider, 1981b). Hence, we expect similar results when using these integrators in the algorithm of Figure 5b. However, these expectations have not been confirmed.

More information is required to determine whether the algorithms of Gallun and Holland (1980) and Sourisseau and Doherty (1980) are worthy of comparative testing.

## APPENDIX A

Normally, the vapor overhead stream from the stripping tower in Figure 6a is small compared with the reflux stream to the azeotropic tower. Hence, to study the dynamic response of azeotropic towers, the stripping tower can be neglected with small errors (Figure 6b). However, our nonlinear programming algorithm to locate steady-state operating conditions (Prokopakis and Seider, 1983) was demonstrated for the configuration in Figure 6a. This Appendix gives the alterations when the stripping tower is eliminated.

Consider the material balances at  $M$  in Figure 6c:

$$f_j = x_{N+1,j}L_{N+1} - x_j^e L^{e'} - rx_j^a L^{a'} - \delta_{j,ent}F_m = 0 \quad j = 1, 2, 3 \quad (A1)$$

where  $\delta$  is the Kronecker delta function. The nonlinear programming problem can be recast as:

$$\underset{V_1, R_{alc}, x_{1,ent}, x_{1,wat}}{\text{minimize}} \quad \phi = \sum_{j=1}^3 f_j^2 \quad P1$$

subject to:

$$\begin{aligned} V_1^L &< V_1 \\ R_{alc}^L &\leq R_{alc} \leq R_{alc}^U \\ 0 &\leq x_{1,ent} \leq x_{1,ent}^U \\ 0 &\leq x_{1,wat} \leq x_{1,wat}^U \\ y_{N,alc}^L &\leq y_{N,alc} \leq y_{N,alc}^U \\ 0 &\leq r \leq 1 \\ 0 &\leq F_m \\ f_j &= 0 \quad j = 1, 2, 3 \end{aligned}$$

The bounds on  $y_{N,alc}$  are sufficient to locate the vapor overhead composition in the feasible window since  $y_{N,ent}$  falls within the narrow band surrounding the ternary azeotrope without inequality constraints. The equality constraints are redundant, but we have found that they significantly increase the rate of convergence with Powell's algorithm (1977).

For each set of design variable values we solve the MESH equations, tray-by-tray, beginning at the bottom of the tower, giving  $V_N$ ,  $y_N$ ,  $L_{N+1}$ , and  $x_{N+1}$ . The vapor overhead stream is adjusted to the temperature of the decanter and split into two liquid phases at equilibrium, giving  $L^{e'}$ ,  $x_j^e$ ,  $L^{a'}$ , and  $x_j^a$ . Then, Eqs. A1 are solved for  $r$  and  $F_m$ , which is accomplished by solution of:

$$\underset{r, F_m}{\text{minimize}} \quad \phi = \sum_{j=1}^3 f_j^2 \quad P2$$

The stationarity conditions are  $\partial\phi/\partial r = \partial\phi/\partial F_m = 0$  and, with analytical differentiation, these give

$$r = \frac{\sum_{j=1}^3 (x_{N+1,j}L_{N+1} - x_j^e L^{e'})x_j^a}{\sum_{j=1}^3 (x_j^a)^2 L^{a'}} \quad (A2)$$

$$F_m = x_{N+1,ent}L_{N+1} - x_{ent}^e L^{e'} - rx_{ent}^a L^{a'} \quad (A3)$$

## Reformulation of P1

To have all variables near unity, scaled variables are introduced:

$$\begin{aligned} X_{1,ent} &= x_{1,ent}/x_{1,ent}^U \\ X_{1,wat} &= x_{1,wat}/x_{1,wat}^U \\ V_1 &= V_1/V_1^L \end{aligned} \quad (A4)$$

and P1 is restated:

$$\underset{V_1, R_{alc}, X_{1,ent}, X_{1,wat}}{\text{minimize}} \quad \phi = \sum_{\substack{j=1 \\ j \neq ent}}^3 f_j^2 \quad P3$$

subject to:

$$\begin{aligned} h_1 &= V_1 - 1 \geq 0 \\ h_2 &= (R_{alc} - R_{alc}^L)(R_{alc}^U - R_{alc}) \geq 0 \\ h_3 &= X_{1,ent}(X_{1,ent}^U - X_{1,ent}) \geq 0 \\ h_4 &= X_{1,wat}(X_{1,wat}^U - X_{1,wat}) \geq 0 \\ h_5 &= (y_{N,alc} - y_{N,alc}^L)(y_{N,alc}^U - y_{N,alc}) \geq 0 \\ h_6 &= r(1 - r) \geq 0 \\ h_7 &= F_m \geq 0 \\ g_j &= f_j = 0 \quad j = 1, 2, 3; \quad j \neq ent \end{aligned}$$

Powell's algorithm (1977) is used to solve P3.

## APPENDIX B

For the ethanol-benzene-water system, vapor pressures were estimated with the Antoine equation using the parameters of Gmehling and Onken (1977), liquid phase activity coefficients with the UNIQUAC equation using the parameters of Prausnitz and coworkers (1980), and heat capacities with a fourth degree polynomial in  $T$  using the parameters of Reid and coworkers (1977). These parameters are given by Prokopakis and Seider (1983) in Table 1.

Data for the system, isopropanol-cyclohexane-water-isopropyl-ether-acetone, were provided by J. Baldwin (1979) and are given by Prokopakis and coworkers (1981a). Vapor pressures were estimated with the extended Antoine equation, liquid-phase activity coefficients with the NRTL equation, and heat capacities with a fourth-degree polynomial in  $T$ .

## ACKNOWLEDGMENT

Helpful conversations were held with Charles W. White, III, and Gary D. Fisher and are acknowledged. Computing time was provided by the School of Engineering and Applied Science at the University of Pennsylvania and is appreciated.

## NOTATION

$a, b$	= parameters in semi-implicit Runge-Kutta method
$A, B$	= parameters in Boston and Sullivan algorithm (Figure 4a)
$A_i$	= active cross-sectional area of Tray $i$ , $\text{m}^2$
$\underline{B}, \underline{C}, \underline{D}, \underline{E}$	= bidiagonal coef. matrices
$C$	= number of chemical species
$\underline{d}_x, \underline{d}_M, \underline{d}_E$	= vectors
$f_j$	= function; $dy/dt$ in Eqn. 16
$f_i^h$	= $dh_i^L/dt$ , Eq. 13
$f_i^M$	= $dM_i/dt$ , Eq. 2

$F_i$	= flow rate of feed to Tray $i$ , mol/s
$g$	= acceleration due to gravity, m/s <sup>2</sup>
$\underline{C}_j$	= tridiagonal coefficient matrix for species $j$
$\underline{C}^d$	= volume of decanter hold-up, m <sup>3</sup>
$h$	= step size; enthalpy, J/mol; inequality residuals (P3, Appendix A)
$H_{w_i}$	= height of weir on Tray $i$ , m
$\underline{I}$	= identity matrix
$\underline{J}$	= Jacobian matrix
$\underline{k}_j$	= increment functions in semi-implicit Runge-Kutta method
$K_j^d$	= liquid-liquid distribution coefficient for species $j$ in decanter
$K_{ij}$	= vapor-liquid distribution coefficient for species $j$ on Tray $i$
$L_i$	= liquid flow rate from Tray $i$ , mol/s
$L_{w_i}$	= length of weir on Tray $i$ , m
$m$	= number of ODE's
$M_i$	= liquid holdup on Tray $i$ , mol
$\underline{M}_L$	= Diagonal hold-up matrix, $(\partial M_i / \partial L_i)$
$\underline{N}$	= number of trays
$P_i$	= pressure on Tray $i$ , bar
$q$	= number of columns in Nordsieck array
$Q_i$	= heat transfer to Tray $i$ , J/s
$r$	= order of accuracy of the GEAR backward difference formula; recycle bypass fraction
$R$	= reflux ratio, $r/(1-r)$
$R_{alc}$	= fraction of alcohol recovered in the azeotropic tower
$R'$	= boil-up ratio, $V_1/L_1$
$s_i$	= fraction of stream in sidedraw from Tray $i$
$t$	= time, s
$T_i$	= temperature of Tray $i$ , K
$\underline{u}$	= matrix of volatility parameters in Boston and Sullivan algorithm (Figure 4a)
$V_i$	= flow rate of vapor stream from Tray $i$ , mol/s
$V_1$	= dimensionless boil-up rate (Eq. A4)
$w_j$	= weighting factors in semi-implicit Runge-Kutta methods
$x_{ij}$	= mole fraction of species $j$ in liquid on Tray $i$
$X$	= see Eq. A4
$y$	= dependent variable
$y_{ij}$	= mole fraction of species $j$ in vapor on Tray $i$
$z_{ij}$	= mole fraction of species $j$ in feed stream to Tray $i$
$\underline{z}$	= Nordsieck array ( $m \times q$ )

#### Greek Symbols

$\alpha_i, \beta_{-1}$	= parameters in GEAR backward difference formulas
$\beta$	= fraction of entrainer phase leaving decanter
$\gamma_\infty$	= characteristic root of Eqs. 26-28 as $h \lambda  \rightarrow \infty$
$\gamma_j$	= liquid-phase activity coefficient for species $j$
$\Delta_{w_i}$	= liquid height over weir on Tray $i$ , m
$\theta, \kappa$	= bounds in inequalities, Eqs. 33-35
$\lambda$	= Eigenvalue
$\bar{\lambda}_s$	= pseudo-eigenvalue for stiff variable (defined by Eq. 29)
$\rho_i^L$	= density of liquid on Tray $i$ , kg/m <sup>3</sup>
$\phi$	= see $P1$ (Appendix A)

#### Subscripts

$0$	= initial value at $t = 0$
$i$	= tray number, reboiler = Tray 1
$j$	= species counter
$L$	= $C + 1$
$m$	= entrainer make-up stream
max	= maximum
$n$	= step counter
$s$	= stiff variable

#### Superscripts

$a$	= aqueous phase leaving decanter
$c$	= condenser
$d$	= decanter
$e$	= entrainer phase leaving decanter
$F$	= feed
$L$	= liquid; lower bound
$s$	= stripping tower
$U$	= upper bound
$v$	= vapor
$-$	= pseudo
$\wedge$	= steady state
$\cdot$	= refers to configuration in Figure 6c

#### LITERATURE CITED

Baldwin, J., Private Communication (1979).

Ballard, D. M., and C. B. Brosilow, "Dynamic Simulation of Multicomponent Distillation Columns," Annual Meeting of AIChE, Miami (Nov., 1978).

Boston, J. F., H. I. Britt, S. Jirapongphan, and V. B. Shah, "An Advanced System for the Simulation of Batch Distillation Operations," *Foundations of Computer-Aided Chemical Process Design*, Eds., R. S. H. Mah and W. D. Seider, AIChE (1981).

Boston, J. F., and S. L. Sullivan, Jr., "A New Class of Solution Methods for Multicomponent, Multistage, Separation Processes," *Can. J. of Chem. Eng.*, **52**, 1 (1974).

Bui, T. D., "Solving Stiff Differential Equations in the Simulation of Physical Systems," *Simulation*, **37** (Aug., 1981).

Distefano, G. P., "Mathematical Modeling and Numerical Integration of Multicomponent Batch Distillation Equations," *AIChE J.*, **14**, 190 (1968a).

Distefano, G. P., "Stability of Numerical Integration Techniques," *AIChE J.*, **14**, 946 (1968b).

Gallun, S. E., and C. D. Holland, "Extractive Distillation Column Described at Unsteady State Using Gear's Procedure," Annual Meeting of AIChE, Chicago (Nov., 1980).

Gmehling, J., and U. Onken, *Vapor-Liquid Equilibrium Data Collection*, DECHEMA, Chemistry Data Series, I, Part 1, Verlag & Druckerei Friedrich Bischoff, Frankfurt (1977).

Hindmarsh, A. C., "GEAR: Ordinary Differential Equation System Solver," Lawrence Livermore Laboratory Report UCID-30001, Rev. 3 (1974).

Howard, G. M., "Unsteady-State Behaviour of Multicomponent Distillation Columns," *AIChE J.*, **16**, 1022 (1970).

Huckaba, C. E., F. P. May, and F. R. Franke, "An Analysis of Transient Conditions in Continuous Distillation Operations," *Chem. Eng. Prog. Symp. Ser.*, No. 46, **59**, 38 (1963).

Huckaba, C. E., F. R. Franke, F. P. May, B. T. Fairchild, and G. P. Distefano, "Experimental Confirmation of a Predictive Model for Dynamic Distillation," *Chem. Eng. Prog. Symp. Ser.*, No. 55, **61**, 126 (1965).

Kim, C., and J. C. Friedly, "Approximate Dynamic Modelling of Large Staged Systems," *IEC Proc. Des. Dev.*, **13**, 177 (1974).

Luyben, W. L., V. S. Verneuil, Jr., and J. A. Gerster, "Experimental Transient Response of a Pilot-Plant Distillation Column. Part IV: Response of a Ten-Tray Column," *AIChE J.*, **10**, 357 (1964).

Magnussen, T., M. L. Michelsen, and A. Fredenslund, "Azeotropic Distillation Using UNIFAC," *Inst. Chem. Eng. Symp. Ser.*, No. 56, Third Int'l. Symp. on Distillation, ICE, Rugby, Warwickshire, England (1979).

Mah, R. S., S. Michaelson, and R. W. H. Sargent, "Dynamic Behaviour of Multicomponent Multistage Systems," *Chem. Eng. Sci.*, **17**, 619 (1962).

Peiser, A. M., and S. S. Grover, "Dynamic Simulation of a Distillation Tower," *Chem. Eng. Prog.*, **58**, 65 (1962).

Powell, M. J. D., "A Fast Algorithm for Nonlinearly Constrained Optimization Calculations," Dundee Conf. on Numerical Analysis (1977).

Prausnitz, J. M., T. F. Anderson, E. A. Grens, C. A. Eckert, R. Hsieh, and J. P. O'Connell, *Computer Calculations for Multicomponent Vapor-Liquid and Liquid-Liquid Equilibria*, Prentice-Hall (1980).

Prokopakis, G. J., B. A. Ross, and W. D. Seider, "Azeotropic Distillation Towers with Two Liquid Phases," *Foundations of Computer-aided Chemical Process Design*, Eds., R. S. H. Mah and W. D. Seider, AIChE (1981a).

Prokopakis, G. J., and W. D. Seider, "Adaptive Semi-Implicit Runge-Kutta Algorithm for the Solution of Stiff Ordinary Differential Equations," *IEC Fund.*, **20**, 255 (1981b).

Prokopakis, G. J., and W. D. Seider, "Feasible Specifications in Azeotropic

Distillation," *AIChE J.*, **29**, No. 1, 49 (1983).  
 Reid, R. C., J. M. Prausnitz, and T. K. Sherwood, *Properties of Gases and Liquids*, 3rd Ed., McGraw-Hill (1977).  
 Rosenbrock, H. H., "Some General Implicit Processes for the Numerical Solution of Differential Equations," *Comp. J.*, **5**, 329 (1963).  
 Seider, W. D., C. W. White, III, and G. J. Prokopakis, "Stiff Ordinary Differential Equations in Chemical Process Analysis," Proceedings of the AIChE-CIESC Meeting in Beijing, China (1982).  
 Sourisseau, K. D., and M. F. Doherty, "Dynamic Simulation of Stiff Distillation Systems," J.A.C.C., San Francisco (1980).  
 Tyreus, B. D., W. L. Luyben, and W. E. Schiesser, "Stiffness in Distillation Models and the Use of an Implicit Integration Method to Reduce Computation Times," *I&EC Proc. Des. Dev.*, **14**, 427 (1975).  
 Waggoner, R. C., and C. D. Holland, "Solution of Problems Involving Conventional and Complex Distillation Columns at Unsteady-State Operation," *AIChE J.*, **11**, 112 (1965).

*Manuscript received March 3, 1982; revision received December 15, and accepted January 6, 1983.*

# Sedimentation of Multisized Particles in Concentrated Suspensions

A model is developed for predicting the sedimentation velocity in suspensions of multisized nonflocculating solids, in which the retarding effect of the smaller particles on the settling velocities of the larger ones is taken into account. Tests of the model, and comparisons with other models, demonstrate that it provides improved prediction of data on suspensions comprising both discrete particle size mixtures and continuous size distributions, and that it is applicable to continuous countercurrent solid-liquid operations.

**M. S. SELIM**

Department of Chemical and Petroleum-  
Refining Engineering  
Colorado School of Mines  
Golden, CO 80401

**A. C. KOTHARI**

Haldor Topsoe, Inc., Houston, TX 77058  
and

**R. M. TURIAN**

Department of Chemical Engineering  
University of Illinois at Chicago  
Chicago, IL 60680

## SCOPE

Sedimentation in concentrated suspensions of particles is a broad subject because of the wide range of particle sizes, the variety of particle shapes, and the complex nature of the hydrodynamic and physicochemical phenomena which govern particle-fluid and particle-particle behavior. The present work is limited to investigation of settling in concentrated noncolloidal suspensions of spherical particles of mixed sizes. Therefore, the important class of flocculant suspensions, usually comprised of particles in the submicron-size range, is excluded. Even with this circumscription the problem is substantial.

Sedimentation in noncolloidal suspensions comprised of spheres of uniform size and density has been investigated extensively. Theoretical results relating the settling velocity to solids volume fraction for such monodisperse suspensions of spheres have been treated in the dilute limit (Smoluchowski, 1912; Burgers, 1941, 1942; Uchida, 1949; McNow and Lin, 1952; Happel, 1958; Kawaguti, 1958; Hasimoto, 1959; Pyun and Fixman, 1964; and Batchelor, 1972). The intermediate and the high-concentration limits are more important in practice, but

less amenable to rigorous theoretical treatment; they have been investigated rather extensively experimentally. Reliable empirical methods for determining the settling velocity-volume fraction (or voidage) relationship for concentrated suspensions of rigid spheres of uniform size and density are available (Garside and Al-Dibouni, 1977).

The subject of sedimentation involving suspensions containing mixed particle sizes is not as well developed, and reliable relationships have not been available. This paper is concerned with development of methods for predicting the settling velocity-voidage relationship in suspensions consisting of discrete as well as continuous mixtures of particle sizes. The method is based on knowledge of the sedimentation behavior of the individual size fractions within the mixture each settling alone in the suspending liquid. Interaction effects among particles of different sizes are accounted for by viewing the sedimentation of a given size fraction to take place in a matrix composed of the suspending fluid and the more slowly settling particles of smaller sizes.

## CONCLUSIONS AND SIGNIFICANCE

Operations involving relative motion between a fluid and suspended particles arise often and include sedimentation, fluidization and co- or countercurrent solid-liquid operations.

The hydrodynamics of slow vertically flowing liquid-particle mixtures, involving noncolloidal particles of uniform size and density, are understood in the dilute limit and can now be reliably treated empirically in the intermediate and concentrated limits. The presence of particles of mixed sizes enhances in-

Correspondence concerning this paper should be addressed to M. S. Selim.